Ultramicroscopy 210 (2020) 112919

Contents lists available at ScienceDirect

Ultramicroscopy

journal homepage: www.elsevier.com/locate/ultramic

Simultaneous multi-region background subtraction for core-level EEL spectra

Jacob T. Held*, Hwanhui Yun, K. Andre Mkhoyan*

Department of Chemical Engineering and Materials Science, University of Minnesota, Minneapolis, MN 55455, United States

ARTICLE INFO

Keywords:
EELS
STEM
Core-Level
Background
Fitting

ABSTRACT

We present a multi-region extension of power law background subtraction for core-level EEL spectra to improve the robustness of background removal. This method takes advantage of the post-edge shape of core-loss EEL edges to enable simultaneous fitting of pre- and post-edge background regions. This method also produces simultaneous and consistent background removal from multiple edges in a single EEL spectrum. The stability of this method with respect to the fitting energy window and the EELS signal to noise ratio is also discussed.

1. Introduction

An important step in the preparation of core-level electron energy-loss (EEL) spectra for analysis and quantification in scanning transmission electron microscopy (STEM) is the removal of the background under the edge of interest. The common practice for removing the background from core-loss edges is to fit a 10–30 eV pre-edge window with a single power law of the form $f(E) = AE^{-r}$, where A is a scaling coefficient and r defines the curvature of the background [1]. The fit curve is then extrapolated and subtracted from the spectrum, leaving background-free core-loss features.

This approach generally works well for thin samples (minimizing bulk plasmon and multiple scattering contributions) with high signal-to-noise core-loss edges above 100 eV (beyond the strong influence of the bulk plasmon) that do not overlap with other signals. However, in many cases, these conditions are not met, resulting in poor estimation of the background [2]. Some of these issues have been addressed in previous studies. For example: Tenailleau et al. [3] introduced a modified function that produced a better fit to fit the tail of the bulk plasmon for background-subtracting low-energy core-loss edges; Egerton et al. [4] presented multiple background fitting models that considered both the pre- and post-edge regions; Verbeek et al. [5,6] introduced a model based quantification of EELS spectra; and Cueva et al. [7] discussed the use of a sum of power laws with fixed exponent values to quickly fit the backgrounds of EELS spectrum images.

Despite these strides in EELS background subtraction, the established tools are often inadequate to use with noisy spectra containing multiple core-loss edges with limited pre-edge regions, which are common in STEM-EEL spectra. In this study, we present a solution to these challenges using a multi-region background fitting method that builds on the approaches presented by Egerton [4] and provides simultaneous and robust background subtraction of all separable edges in the spectrum.

2. Method

Just as the pre-edge background under a core-loss EEL edge is well represented by a power law [1], the post-edge region, beyond any significant extended-loss features, obeys the same functional form [4,8]. This behavior is consistent with Bethe theory [9–11], and the value of r is generally between 1 and 6 under typical EELS acquisition conditions [7,8,10]. However, the value of r may be different in the pre- and post-edge regions and it is dependent on several factors including the EELS acceptance angle, the mass thickness of the sample, and the ionization edge [10].

In the method presented here, the power law behavior of the post-edge region constrains and refines the background fitting function for every EEL edge in a spectrum by simultaneously fitting both the pre- and post-edge energy windows with interdependent functions. Applying this to an isolated EEL edge, the pre-edge background follows a single power law:

$$f_1(E) = A_1 E^{-r_1} \quad E \in R_1, \tag{1}$$

and the post-edge follows:

$$f_2(E) = f_1(E) + A_2 E^{-r_2} \quad E \in R_2, \tag{2}$$

where f_1 is fit to a 10–30 eV energy window R_1 prior to the edge onset and f_2 is fit to a post-edge energy window R_2 beyond significant edge

* Corresponding authors.
E-mail addresses: heldx123@umn.edu (J.T. Held), mkhoyan@umn.edu (K.A. Mkhoyan).

https://doi.org/10.1016/j.ultramic.2019.112919
Received 11 June 2019; Received in revised form 6 November 2019; Accepted 13 December 2019
Available online 14 December 2019
0304-3991/

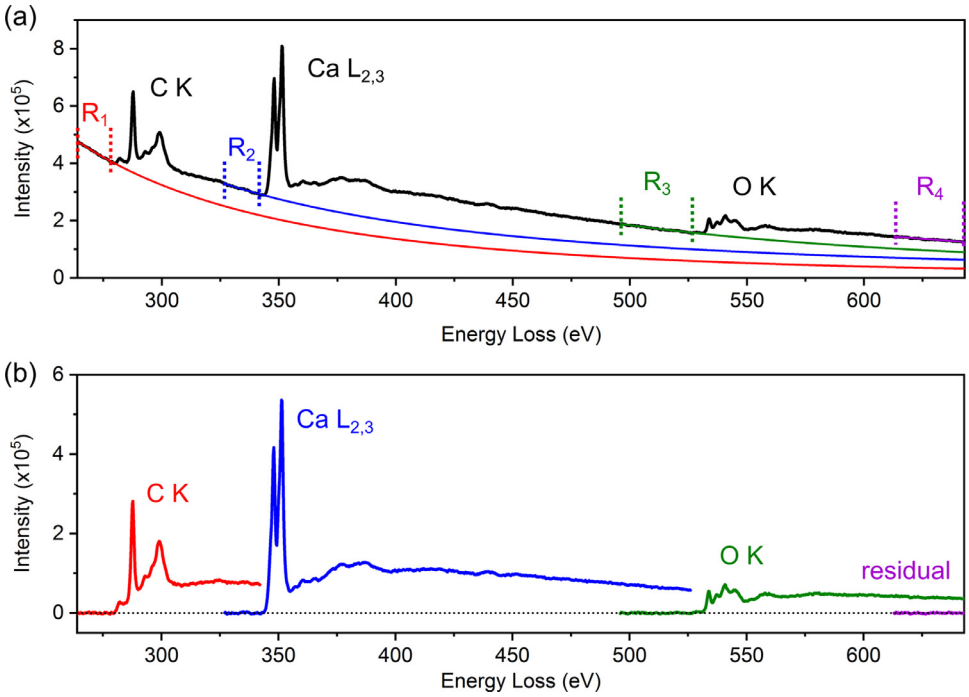

Fig. 1. Multi-region background subtraction of C *K*, Ca $L_{2,3}$, and O K-edges of calcite in a single EEL spectrum. (a) Raw spectrum (black) showing the background fitting windows (R_i within the dotted vertical lines) and the corresponding extrapolated fits (solid red, blue, green, and purple curves). (b) C *K*, Ca $L_{2,3}$, and O *K*-edges as well as the residual from energy window R_4 after background subtraction. (For interpretation of the references to colour in this figure legend, the reader is referred to the web version of this article.)

features.

For an EEL spectrum containing m core-loss EEL edges, a total of $n = m + 1$ energy windows must be fit (one pre-edge window for each edge and a final window following the highest-energy edge). The pattern in Eqs. (1) and (2) is extended to accommodate additional edges by adding a power law term to the fitting function in each subsequent energy window. Accordingly, the function fit to the jth energy window is:

$$f_j(E) = \sum_{i=1}^{j} A_i E^{-r_i} \quad E \in R_j, \tag{3}$$

such that the full piecewise fitting function is:

$$F(E) = \begin{cases} f_1(E) & E \in R_1 \\ f_2(E) & E \in R_2 \\ \vdots & \\ f_n(E) & E \in R_n \end{cases}. \tag{4}$$

All A_i and r_i are then optimized simultaneously by minimizing the sum-squared error across all windows. This is accomplished with a numerical optimization algorithm such as Nelder–Mead [12,13]. It is worth noting that, due to the large values of A_i, it is useful to replace A_i with $a_i = ln(A_i)$.

During fitting, A_i and r_i are subject to constraints:

$$A_i \geq 0, \tag{5}$$

ensuring the fit function is positive, and

$$1 \leq r_i \leq 6, \tag{6}$$

ensuring a physical power law shape within expected bounds [7,8,10]. These constraints prevent negative intensities or positive slopes in the post-edge region. After fitting, each background function $f_i(E)$ is extrapolated from the starting point of R_i and subtracted from the original spectrum, producing background-subtracted spectra for each EEL edge. If this method is applied to only one edge and force the exponents r_i to be equal in the pre- and post-edge regions, it turns into the simpler method described by Egerton [4].

Fig. 1 shows an example of the application of this method to an EEL spectrum obtained from a sample of crushed natural calcite ($CaCO_3$). EEL spectra were acquired from a thin region of the sample over vacuum in an FEI Titan G2 60–300 STEM, operated at 200 kV with a probe semi-convergent angle of 24 mrad and an EEL spectrometer collection angle of 29 mrad. An energy range of 213–724 eV with a 0.25 eV dispersion was used here to capture the C *K*, Ca $L_{2,3}$, and the O *K* edges in a single spectrum. The background fitting windows $R_1 = 264 - 279$ eV (pre-C *K*), $R_2 = 327 - 342$ eV (pre-Ca $L_{2,3}$), $R_3 = 496 - 526$ eV (pre-O *K*), and $R_4 = 613 - 643$ eV (post-O *K*) were used, producing a simultaneous background fit for all three edges. For this spectrum, the optimized parameters were: $a_1 = 30.4$, $r_1 = 3.08$; $a_2 = 19.3$, $r_2 = 1.39$; $a_3 = 36.2$, $r_3 = 3.99$; $a_4 = 32.2$, $r_4 = 3.35$.

In this method, according to Eq. (3), every additional background fitting window adds two more parameters (r_i and A_i) that must be optimized. For spectra with many edges, and therefore many background fitting regions, this adds computational time. It is, therefore, very useful to establish good initial guesses for each parameter. In the case of a well-characterized experimental setup and known sample mass-thickness, reasonable initial guesses for the $r_i^{(0)}$ values can be estimated [8]. In situations where experimental conditions cannot be used to generate the initial guesses for $r_i^{(0)}$, a coarse fit may be performed with tighter constraints than the final optimization by fitting each window sequentially and independently: $A_1^{(0)}$ and $r_1^{(0)}$ are fit over R_1 (Eq. (1)), then, holding these values constant, $A_2^{(0)}$ and $r_2^{(0)}$ are fit over R_2 (Eqn. 2), etc. This sequential fitting procedure yields $A_i^{(0)}$ and $r_i^{(0)}$, which can then be used as initial guesses in the full, simultaneous, optimization of all parameters in the multi-region fit.

While the sequential fit is inherently subject to the same issues as 1-region power law fits because each region is independently optimized, it offers a good set of initial guesses and can dramatically reduce the computational time of the multi-region fit. The multi-region fit will have an overall fitting error less than (or equal to) that of the sequential fit, but the local error in each region may increase or decrease. Because the background fits for each EEL edge are interdependent and simultaneously optimized, a multi-region fit offers increased stability over a 1-region fit, making it less sensitive to the SNR of the data and the size of the fitting window(s).

To demonstrate this improved stability, the spectrum shown in Fig. 1 was fit with varying fitting window sizes for each R_i. Here, the lower energy limit of the fitting window was changed while the upper limit and the rest of the windows were fixed. The fit was optimized for

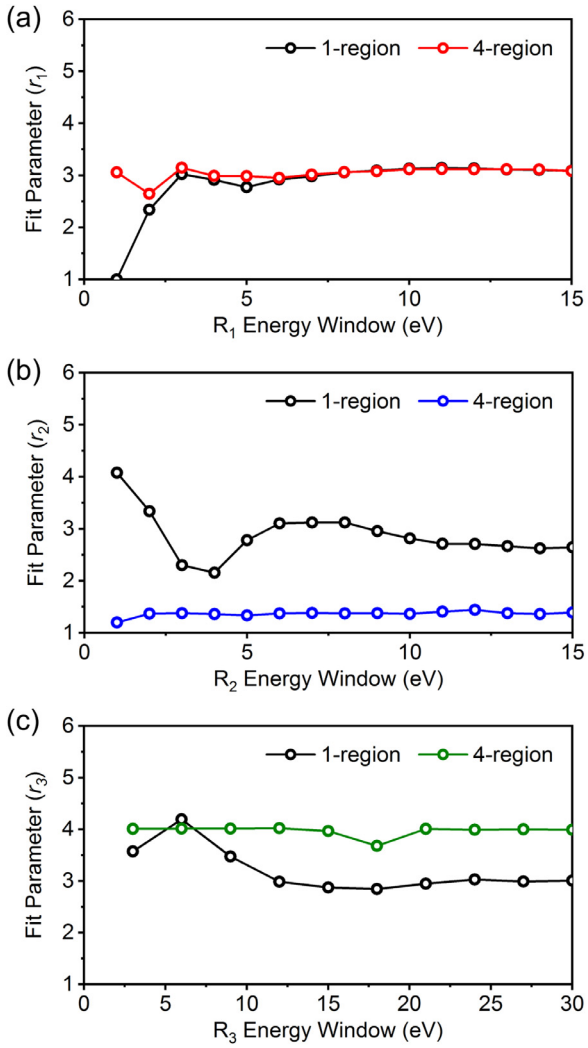

Fig. 2. Sensitivity of 1- and 4-region background fits to the size of fitting window (R_i) for the spectrum shown in Fig. 1. (a) Values of fitting parameter r_1 for various sizes of energy window R_1. The 1-region fit is shown in black; r_1, the corresponding fitting parameter from the 4-region fit is shown in red. (b, c) The procedure from (a) repeated for each of the pre-edge regions of the 4-region fit, showing the 1-region r and the analogous 4-region r_i. (For interpretation of the references to colour in this figure legend, the reader is referred to the web version of this article.)

each case. This was repeated for a 1-region fit over each of the energy windows, and the resultant values of r_i for each case were compared (see Fig. 2). It is important to note that, aside from the value of r_1 in Fig. 2a, the absolute values of r_i obtained from the multi-region fit cannot be directly compared with the 1-region fit because the fitting function is not the same; the multi-region fit is a sum of multiple power laws, while the single-region fit is only a single power law. However, the variance of the r_i values directly relates to the stability of the fit.

Even when one fitting window of the multi-region fit is very small ($<$ 10 eV, or $<$ 40 data points), the fit remains stable due to the influence of the other fitting windows. This stabilizing effect for the multi-region fit is strongest when the extrapolated backgrounds of the lower energy regions account for the majority of the background under subsequent regions, increasing the interdependence of the fits for each region.

We tested the stability of a multi-region fit against two essential parameters, the EELS experimental conditions (exposure time, or SNR), and the number of data points in the fitting window. We examined the simplest case; fitting pre- and post-edge regions of a single edge. Fig. 3 shows the results of sequential and 2-region fits for a Ca $L_{2,3}$ edge obtained under the same conditions as the results shown in Fig. 1 but with exposure times of 0.1 and 5 s, corresponding to signal to noise ratios $SNR_{dB} = 36$ and $SNR_{dB} = 42$. Here SNR with signal powers were used:

$$SNR_{dB} = 10log_{10}(P_s/P_n), \quad (7)$$

where P_s is the power of the pre-edge signal and P_n is the power of the noise in the same region.

In each case, the results of the sequential fits are used as the initial guesses for the 2-region fits as discussed above, and the limits of r_{pre} were extended to 0 to 10. The value of r_{pre} governs the shape of the background function and serves as the key parameter for evaluating the stability of the background fit. When the pre-edge fitting window size was reduced, the sequential and 2-region fits performed similarly down to a certain window size. Further reducing the window size yielded progressively divergent values of r_{pre} in the sequential fit, causing the overall error to increase dramatically as the post-edge region no longer behaved as a power law (Fig. 3c). The multi-region fit remained stable down to the smallest windows considered (1 eV, or 5 data points) due to the stabilization offered by the post-edge region. The window size at which this divergence occurred is larger for the 0.1 s exposure spectrum due to its lower SNR. It should be noted that because r_{pre} is fit to the first region in the sequence, the results of the sequential fit for the pre-edge region are by definition the same as a 1-region fit.

To further evaluate the effects of the window size (number of data points), the fitting procedure was repeated for three different spectra at each exposure time (obtained from adjacent regions on the sample). The fit values of r_{pre} for all window sizes are shown in Fig. 4. As can be seen in Fig. 4, there is considerably more scatter in the fits for the 0.1 s exposure spectra. In both cases, the 2-region fits yielded less variance in the value of r_{pre} (Fig. 4c). Additionally, despite the allowed range of 0 to 10 for r_{pre}, all of the 2-region values were within the accepted range of 1 to 6, while cases of the sequential fit fell well outside this range.

This procedure was repeated to include 1 s and 10 s exposure times. The results are shown in Fig. 4c. In each case studied, the muti-region fit produced a narrower (more stable) distribution of r_{pre} than the sequential fit, and this difference is greater at low SNR. At high SNR, $SNR_{dB} \gtrsim 45$, as seen in Fig. 3c, the fits agree, such that negligible improvement is gained from the full multi-region fit for a single EELS edge.

Under certain conditions, it may be advantageous to add a term or otherwise modify Eq. (3) to account for features beyond the lower range of the spectrum, which can change the shape of the background such that it no longer obeys a simple power law. Depending on the specific conditions of the dataset, such modifications can involve altering the first term, $i = 1$, of Eq. (3) to model the behavior of the bulk plasmon as described by Tenailleau and Martin [3], or including an additional power law term with a fixed r value as described by Cueva et al. [7]. Any modifications made in this way are applied to the fitting functions for all windows in the multi-region fit.

3. Implementation

A multi-region background fit and removal is particularly useful for a STEM-EEL spectrum image or line scan containing multiple core-loss edges. Individual spectra in these datasets are often obtained over very short integration times to mitigate the effects of sample drift and beam damage, resulting in a low SNR. By making effective use of additional regions of the spectrum, a multi-region fit ensures stable behavior of the background fit for every edge in the spectrum. This method facilitates not only better elemental mapping, but also comparison of fine structures in each background-subtracted edge.

A linescan across the interface between $BaSnO_3$ (BSO) and La-doped $SrSnO_3$ (LSSO) provides a good example of such a situation. In this example, a cross-sectional TEM specimen of a BSO/LSSO heterostructure, grown by hybrid molecular beam epitaxy to study

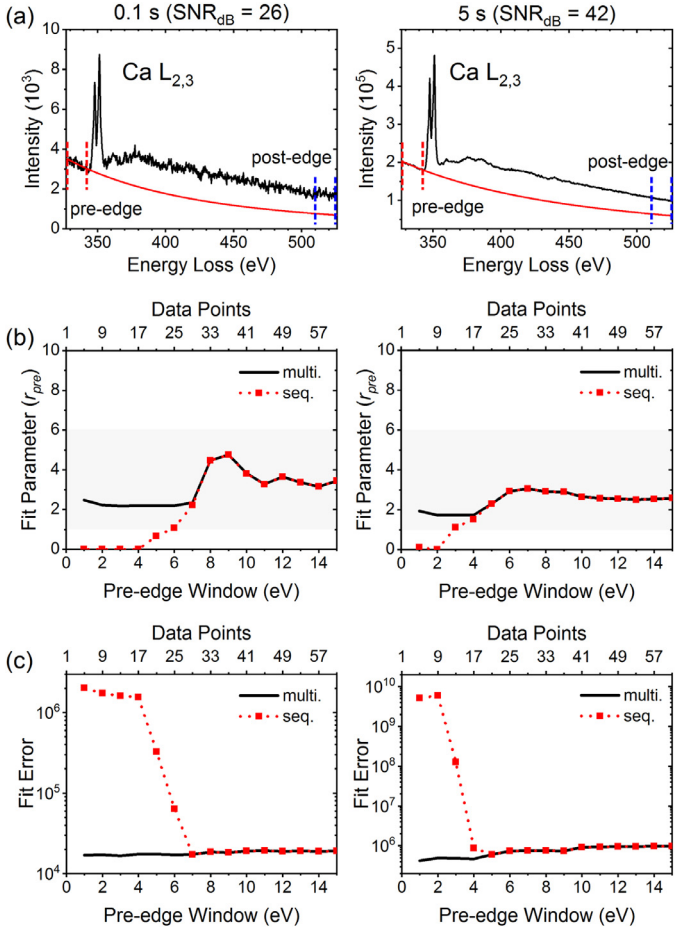

Fig. 3. 2-region vs. sequential background subtraction of a single Ca $L_{2,3}$ edge obtained with exposure times of 0.1 and 5 s. (a) Raw spectra showing pre- and post-edge fitting windows as well as the 2-region fit background. (b) The values of r_1 for the 2-region and sequential fits for varied pre-edge window sizes. The accepted range of r values (1 to 6) is highlighted in grey. (c) Sum-squared error normalized by the total number of fit points for both fitting methods.

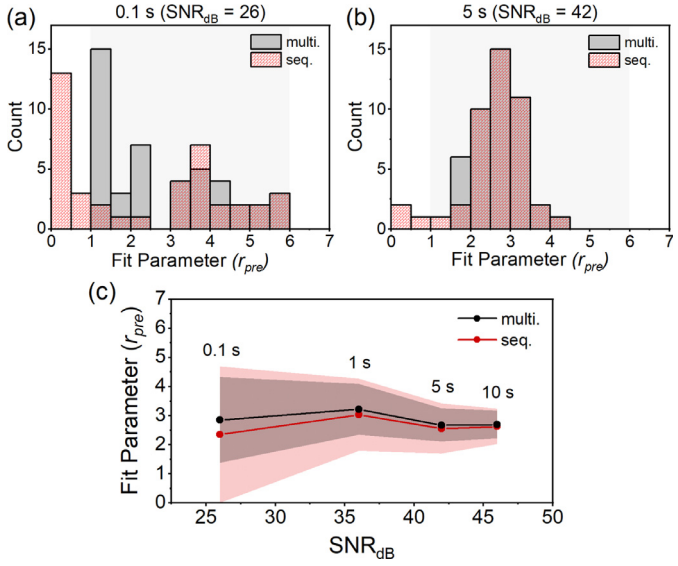

Fig. 4. Values of r_1 from three spectra using the procedure shown in Fig. 3 for (a) 0.1 s, and (b) 5 s exposure times. The accepted range of r values (1 to 6) is highlighted in grey. (c) Mean values of r_{pre} and standard deviations (shaded regions) for different SNR.

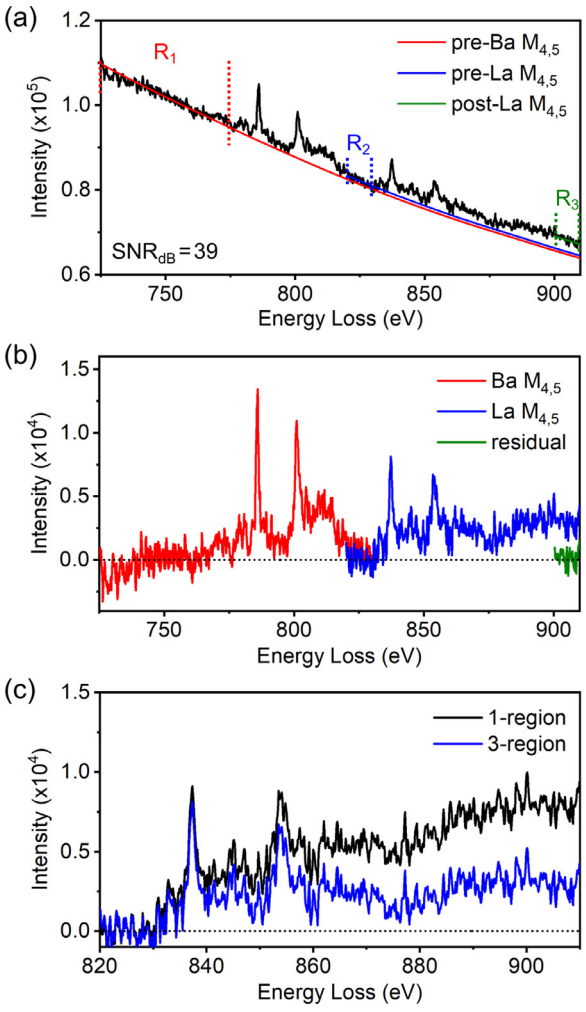

Fig. 5. Background subtraction of Ba and La $M_{4,5}$ edges obtained near the interface between BSO and LSSO. (a) Raw spectrum showing the background fitting windows: R_1 = 725 − 775 eV; R_2 = 820 − 830 eV; R_3 = 900 − 910 eV, and the corresponding fits. (b) Background-subtracted Ba and La $M_{4,5}$ edges. (c) Comparison of the La $M_{4,5}$ edge produced by this 3-region fit with a 1-region fit of R_2.

modulation doping at this interface [14]. was studied. A monochromated-EELS linescan was obtained across the interface of the two materials using an FEI Titan G2 60–300 STEM operated at 200 kV with a semi-convergent angle of 17 mrad, an EEL spectrometer collection angle of 29 mrad. A spectrum from the data set is shown in Fig. 5.

The shape and intensity of the La $M_{4,5}$ edges were of particular interest for the analysis of this sample because they are used to determine the concentration and location of La dopants across the interface. In this case, there were multiple factors that had to be considered: the La and Ba $M_{4,5}$ edges exhibited a low SNR, SNR_{dB} = 39; the pre-La $M_{4,5}$ region R_2 is relatively small (10 eV) and lies within the extended-loss features of the Ba $M_{4,5}$ edge. The pre-Ba $M_{4,5}$ background was also influenced by the extended-loss features of the Sn $M_{2,3}$ edge. To overcome these challenges, we used a modified 3-region fit with background fitting windows: R_1 = 725 − 775 eV; R_2 = 820 − 830 eV; R_3 = 900 − 910 eV.

A standard Sn extended-loss spectrum from intrinsic $SrSnO_3$ was background-subtracted and included as an additional term, $A_{Sn}I_{Sn}^{(ref)}$, in the background fitting function. This extra term necessitated a larger window for R_1 to capture as much of the Sn character as possible and ensure a stable fit. This modified 3-region background fit was used to remove the background from the Ba and La $M_{4,5}$ edges (Fig. 5). For comparison, a 1-region fit for the background under the La $M_{4,5}$ edge

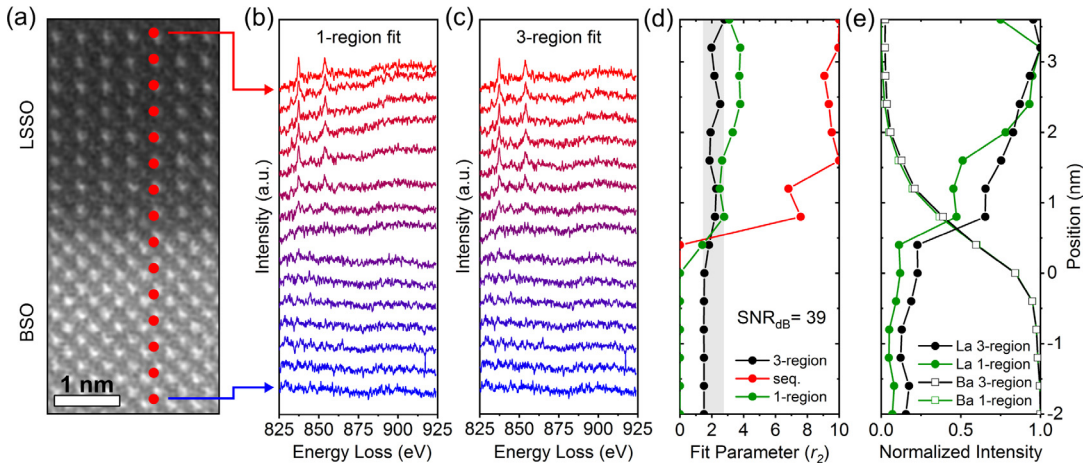

Fig. 6. STEM-EELS line scan across the interface between BSO and LSSO. (a) HAADF-STEM image of the region of interest with red dots indicating the approximate locations of each data point in the line scan. (b) La $M_{4,5}$ edges for each point on the line scan using 1-region background subtraction. (c) La $M_{4,5}$ edges for each point on the line scan using the 3-region background subtraction shown in Fig. 5. (d) Values of r_2 (pre-La $M_{4,5}$) at for each spectrum using single-region, sequential, and 3-region fits. The range of the r_3 values from the 3-region fit is highlighted in grey. (e) Normalized intensities of Ba $M_{4,5}$ and La $M_{4,5}$ edges obtained by scaling standard spectra to the background-subtracted edges using 1- and 3-region background subtraction. (For interpretation of the references to colour in this figure legend, the reader is referred to the web version of this article.)

using the same fitting window R_2 yielded a considerably different and non-physical result (the extended-loss intensity grew rather than obeying a power law), as shown in Fig. 5c.

When extended to the rest of the spectra in the line scan (Fig. 6), the aberrant behavior of the 1-region background subtraction is even more apparent. The R_1 (pre-Ba $M_{4,5}$) fit behaved similarly for the sequential, 1- and 3-region fitting methods, but while the 3-region fit produced a very consistent and sensible shape in the La $M_{4,5}$ edge, the behavior of the 1-region and sequential fits varied significantly along the line scan. Specifically, the 1-region fit over-subtracted the background at the BSO end of the line scan (causing the background-subtracted spectra to be negative) and under-subtracted the background at the LSSO end of the line scan, as discussed for the example in Fig. 5c. The degree of this over- and under- subtraction caused the shape and quantification of the La $M_{4,5}$ edge to vary dramatically between spectra.

To quantify the relative content of La and Ba across the interface while minimizing the influence of noise, a standard La $M_{4,5}$ spectrum was obtained from the LSSO and background-subtracted using the same conditions as the rest of the line scan. This standard was then scaled to the background-subtracted La $M_{4,5}$ edge at each point using linear least squares fitting. This procedure was repeated with the Ba edge to produce the concentration profiles shown in Fig. 6e. Although the 1- and 3-region cases agree well on the Ba profile, the comparative stability of the 3-region background subtraction resulted in a much smoother curve for the La profile.

It is worth noting that for the low-concentration points along the line scan, the 3-region background subtraction case consistently overestimated the concentration of each element, though this was more noticeable for La. This is because the third region R_3 was forced to follow power law behavior to minimize fitting error; that is, it could not be negative, and it had to maintain a negative slope in that region. Lacking such constraints, the 1-region background subtracted spectra for the same points often became negative in the R_3 region. In this case, minor extended loss features from the Ba edge may have exacerbated the issue, but this tendency for a multi-region background fit to undersubtract the background should be taken into consideration when working with low signal-to-noise data.

4. Conclusion

The multi-region background fitting method presented in this study offers more more reliable background subtraction than customary 1-region power law fits, although it is more computationally expensive. By simultaneously fitting the pre- and post-edge regions of each edge in the spectrum with a series of power laws without forcing the pre- and post-edge values of r to be the same, it is consistent with established scattering theory. This method ensures stable behavior of the background-subtracted spectra even for low SNR spectra and spectra with limited background fitting regions. It is particularly well suited for simultaneous fitting of multiple edges because it not only benefits from the additional background regions, but also yields background-subtracted spectra for each edge.

Declaration of Competing Interest

The authors declare that they have no known competing financial interests that could have influenced the work reported in this paper.

Acknowledgments

This work is supported in part by SMART, one of seven centers of nCORE, a Semiconductor Research Corporation program, sponsored by National Institute of Standards and Technology (NIST), and by UMN MRSEC program under award no. DMR-1420013. This work utilized the College of Science and Engineering Characterization Facility, University of Minnesota, supported in part by the NSF through the UMN MRSEC program. H. Y. acknowledges a fellowship from the Samsung Scholarship Foundation, Republic of Korea. J. T. H. acknowledges support from a Doctoral Dissertation Fellowship received from the graduate school at the University of Minnesota.

References

[1] R.F. Egerton, Electron Energy-Loss Spectroscopy in the Electron Microscope, Springer Science & Business Media, 2011.
[2] D.-R. Liu, L. Brown, Influence of some practical factors on background extrapolation in eels quantification, J. Microsc. 147 (1) (1987) 37–49.
[3] H. Tenailleau, J. Martin, A new background subtraction for low-energy eels core edges, J. Microsc. 166 (3) (1992) 297–306.
[4] R.F. Egerton, M. Malac, Improved background-fitting algorithms for ionization edges in electron energy-loss spectra, Ultramicroscopy 92 (2) (2002) 47–56.
[5] J. Verbeeck, S. Van Aert, Model based quantification of EELS spectra, Ultramicroscopy 101 (2004) 207–224.
[6] G. Bertoni, J. Verbeeck, Accuracy and precision in model based EELS quantification, Ultramicroscopy 108 (2008) 782–790.
[7] P. Cueva, R. Hovden, J.A. Mundy, H.L. Xin, D.A. Muller, Data processing for atomic resolution electron energy loss spectroscopy, Microsc. Microanal. 18 (4) (2012)

667–675.
[8] D. Maher, D. Joy, R. Egerton, P. Mochel, The functional form of energy-differential cross sections for carbon using transmission electron energy-loss spectroscopy, J. Appl. Phys. 50 (8) (1979) 5105–5109.
[9] H. Bethe, Zur theorie des durchgangs schneller korpuskularstrahlen durch materie, Annalen der Physik 397 (3) (1930) 325–400.
[10] R. Egerton, K-shell ionization cross-sections for use in microanalysis, Ultramicroscopy 4 (2) (1979) 169–179.
[11] R. Leapman, P. Rez, D. Mayers, K, l, and m shell generalized oscillator strengths and ionization cross sections for fast electron collisions, J. Chem. Phys. 72 (2) (1980) 1232–1243.
[12] J.A. Nelder, R. Mead, A simplex method for function minimization, Comput. J. 7 (4) (1965) 308–313.
[13] W.H. Press, S.A. Teukolsky, W.T. Vetterling, B.P. Flannery, Numerical Recipes 3rd edition: The Art of Scientific Computing, Cambridge University Press, 2007.
[14] A. Prakash, N.F. Quackenbush, H. Yun, J. Held, T. Wang, T. Truttmann, J.M. Ablett, C. Weiland, T.-L. Lee, J.C. Woicik, K.A. Mkhoyan, B. Jalan, Separating electrons and donors in $BaSnO_3$ via band engineering, Nano Lett. 19 (12) (2019) 8920–8927.